Water Research 168 (2020) 115170

Contents lists available at ScienceDirect

Water Research

journal homepage: www.elsevier.com/locate/watres

Achieving arsenic concentrations of <1 μg/L by Fe(0) electrolysis: The exceptional performance of magnetite

C.M. van Genuchten [a, b, *], T. Behrends [a], S.L.S. Stipp [c], K. Dideriksen [b]

[a] Department of Earth Sciences – Geochemistry, Faculty of Geosciences, Utrecht University, Utrecht, 3508TA, the Netherlands
[b] Department of Geochemistry, Geological Survey of Denmark and Greenland, Copenhagen, Denmark
[c] Physics, Technical University of Denmark, Kongens Lyngby, Denmark

ARTICLE INFO

Article history:
Received 17 May 2019
Received in revised form
4 September 2019
Accepted 9 October 2019
Available online 11 October 2019

Keywords:
Electrocoagulation
EXAFS spectroscopy
Arsenic treatment
Mineral formation
Oxyanion incorporation

ABSTRACT

Consumption of drinking water containing arsenic at concentrations even below the World Health Organization provisional limit of 10 μg/L can still lead to unacceptable health risks. Consequently, the drinking water sector in the Netherlands has recently agreed to target 1 μg/L of arsenic in treated water. Unfortunately, in many poor, arsenic-affected countries, the costs and complexity of current methods that can achieve <1 μg/L are prohibitive, which highlights the need for innovative methods that can remove arsenic to <1 μg/L without costly support infrastructure and complicated supply chains. In this work, we used Fe(0) electrolysis, a low cost and scalable technology that is also known as Fe(0) electrocoagulation (EC), to achieve <1 μg/L residual dissolved arsenic. We compared the arsenic removal performance of green rust (GR), ferric (oxyhydr)oxides (Fe(III) oxides) and magnetite (Mag) generated by EC at different pH (7.5 and 9) in the presence of As(III) or As(V) (initial concentrations of 200–11,000 μg/L). Although GR and Fe(III) oxides removed up to 99% of initial arsenic, neither Fe phase could reliably meet the 1 μg/L target at both pH values. In contrast, EC-generated Mag consistently achieved <1 μg/L, regardless of the initial As(V) concentration and pH. Only solutions with initial As(III) concentrations ≥2200 μg/L resulted in residual arsenic >1 μg/L. As K-edge X-ray absorption spectroscopy showed that Mag also sorbed arsenic in a unique mode, consistent with partial arsenic incorporation near the particle surface. This sorption mode contrasts with the binuclear, corner sharing surface complex for GR and Fe(III) oxides, which could explain the difference in arsenic removal efficiency among the three Fe phases. Our results suggest that EC-generated Mag is an attractive method for achieving <1 μg/L particularly in decentralized water treatment.

1. Introduction

Chronic exposure to arsenic in drinking water profoundly impacts human health, causing cancer and death (Kapaj et al., 2006; Naujokas et al., 2013; Rahman et al., 2009), and results in major loss of income for millions of people (Roy, 2008). In the 1990s, the World Health Organization (WHO) revised its recommended limit of arsenic in drinking water from 50 μg/L to the current provisional limit of 10 μg/L (World Health Organization, 2004). The 10 μg/L limit has also been adopted by many regulatory agencies around the world (NHMRC, 2011, SABS, 2001; USEPA, 2006). However, recent research suggests that negative health effects, e.g. excess risk of bladder and kidney cancer (Saint-Jacques et al., 2018) and diabetes (Brauner et al., 2014), can result from chronic exposure to arsenic at levels <10 μg/L. Motivated by cost comparisons between water treatment innovation and arsenic related health impacts, the drinking water sector in the Netherlands has recently agreed to target arsenic concentrations at 1 μg/L (van der Wens et al., 2016; Ahmad et al., 2019). While many other countries suffer from geogenic arsenic contamination, the costs and complexity of current methods to achieve <1 μg/L prohibit targeting similarly low arsenic levels. Consequently, there is a strong need for innovative technologies that can meet the 1 μg/L criterion without major costs, complex support infrastructure and supply chains.

The electrolysis of Fe(0) metal or steel, also known as Fe(0) electrocoagulation (Fe(0) EC), is a promising, cost effective and scalable arsenic treatment method with proven suitability in a

* Corresponding author. Department of Earth Sciences, Geochemistry, Faculty of Geosciences, Utrecht University, Utrecht, 3508TA, the Netherlands.
E-mail address: cvg@geus.dk (C.M. van Genuchten).

https://doi.org/10.1016/j.watres.2019.115170

range of arsenic affected communities (Amrose et al. 2014, 2015). In EC, a low electric current is applied to Fe(0) electrodes in contact with a solution containing arsenic. Electrolysis of Fe(0) produces dissolved Fe(II) at a rate that is controlled by the magnitude of the applied current (Bard and Faulkner, 2001; van Genuchten et al., 2018). The aqueous Fe(II) is then oxidized by dissolved oxygen (O_2) to form insoluble Fe (oxyhydr)oxide precipitates (Lakshmanan et al., 2009; Li et al., 2012). Arsenic removal in Fe(0) EC systems occurs by sorption to these Fe (oxyhydr)oxides (van Genuchten et al., 2012).

While Fe(0) EC is gaining acceptance as a robust arsenic treatment method, its full potential is not yet known because Fe(0) EC is traditionally applied to produce Fe(III) precipitates (Kobya et al., 2016; Kumar et al., 2004; Wan et al., 2011). Since the initial product of Fe(0) electrolysis is Fe(II) (Lakshmanan et al., 2009), mixed valent Fe(II,III) (hydr)oxides, such as magnetite (Mag) and green rust (GR), can form when Fe(II) fluxes are high enough to prevent complete Fe(II) oxidation (van Genuchten et al., 2018). The controlled production of Fe(II,III) (hydr)oxides by Fe(0) EC could lead to significant improvements in arsenic removal performance, partly because of the potential for unique arsenic uptake modes by these minerals (Wang et al. 2010, 2011). For example, arsenite (As(III)) and arsenate (As(V)) have been proposed to substitute for tetrahedral FeO_4 in the Mag structure (Wang et al. 2008, 2011, 2014). This uptake mechanism differs from the typical binuclear, corner sharing arsenic adsorption complex detected for Fe(III) (oxyhydr)oxides (Waychunas et al., 1993). However, the relationship between the arsenic complex and the ability to decrease aqueous arsenic to <1 μg/L has not been investigated.

In addition to the mode of arsenic uptake, the efficiency of arsenic removal by Fe(0) EC is expected to depend on a variety of factors, including the rate of Fe(II) production, the initial arsenic oxidation state and solution pH. The Fe(II) production rate is an important parameter for Fe(0) EC treatment because it controls the type of Fe phase that forms (i.e. Fe(II,III) vs Fe(III) precipitates) (van Genuchten et al., 2018). It can also impact the extent of As(III) oxidation by altering the dynamics of reactive oxidants (Li et al., 2012), i.e. the reaction of Fe(II) with O_2 generates oxidants (Fe(IV)) that can oxidize As(III), but these oxidants can also be quenched by residual Fe(II) (Hug and Leupin, 2003). Because the sorption affinity of negatively charged As(V) for Fe (oxyhydr)oxide surfaces is orders of magnitude higher than As(III) (Roberts et al., 2004), arsenic removal benefits from effective As(III) oxidation. However, As(V) sorption to Fe precipitates depends strongly on pH, decreasing as pH increases above the point of zero charge of the mineral, which contrasts the low pH dependence of As(III) uptake (Dixit and Hering, 2003). Since several co-occurring processes can impact the arsenic removal efficiency, a complete understanding of the potential of Fe(0) EC to achieve <1 μg/L aqueous arsenic requires investigating a range of parameters, including the initial concentration of As(V) and As(III), solution pH and the identity of the Fe phase as controlled by the Fe(II) production rate.

In this work, we compare the arsenic removal performance of GR, Mag and Fe(III) precipitates generated by Fe(0) EC with the purpose of achieving the target of 1 μg/L residual arsenic. Arsenic removal experiments were performed at pH 7.5 and 9 in solutions with 200 to 11,000 μg/L initial As(V) or As(III), which spans the range of typical geogenic arsenic levels (BGS, 2001). The experiments were combined with characterization of the oxidation state and local bonding environment of sorbed arsenic by X-ray absorption spectroscopy (XAS). These results are essential to design the most efficient Fe(0) EC system that meets low target levels of residual arsenic, while considering important secondary criteria, such as electricity consumption, arsenic remobilization from the solids and ease of particle separation from treated water.

2. Methods

2.1. Arsenic removal experiment using Fe(0) EC

For the arsenic removal experiments, we followed the synthesis procedures for GR, Fe(III) precipitates and Mag by Fe(0) EC reported in our previous work (van Genuchten et al., 2018). Experiments were performed in Teflon reactors, using 200 mL electrolyte solutions at room temperature open to the atmosphere. The EC cell consisted of Fe(0) electrodes with 10 cm^2 submerged surface area, spaced ~1 cm apart. The solution compositions were similar to those previously reported (van Genuchten et al., 2018), with all solids generated in 10 mM sodium chloride background electrolyte and solutions for GR experiments also containing 2 mM carbonate. We used 10 mM NaCl as an inert background electrolyte to ensure our solutions had similar ionic strength as groundwater in arsenic-affected regions of South Asia (BGS, 2001). We note that orders of magnitude lower chloride concentrations could be used with negligible impact on the efficiency of Fe(II) production by EC (van Genuchten et al., 2017). The initial As(III) or As(V) concentrations ranged from 200 to 11,000 μg/L. Mixtures of $N_{2(g)}$ and air were used to set the initial O_2 at 3.0 mg/L, which was measured with a Hach LDO optical probe. Experiments were performed at pH of 7.5 and 9.0 to cover a typical range of pH for groundwaters contaminated by arsenic (BGS, 2001). The initial pH was set using dilute HCl or NaOH.

Arsenic removal experiments were initiated by applying a galvanostatic current to the Fe(0) EC cell. A total of 3 mM Fe (168 mg Fe/L, 600 C/L by Faraday's law) was generated in each experiment, using an iron(II) production rate (IPR) of 300 μM/min (current of 200 mC/s) to generate Fe(II,III) phases and 30 μM/min (current of 20 mC/s) to form Fe(III) precipitates. At these IPRs, the GR and Mag experiments required shorter electrolysis time (10 min) than the Fe(III) precipitate experiments (100 min). The 3 mM total Fe (168 mg Fe/L) generated by EC in our experiments was selected to be consistent with the Fe concentration added in existing EC field treatment of arsenic contaminated groundwater in West Bengal, India (Amrose et al., 2014; Müller et al., 2019). This 3 mM Fe (168 mg Fe/L) corresponds to As/Fe ratios of 0.1–5 mol%. During electrolysis, pH was adjusted manually, where needed, to maintain the initial value using dilute HCl or NaOH, which is not typically performed in field Fe(0) EC treatment but was required in our experiments to interpret the impact of pH on our results. The DO was allowed to drift in response to Fe(II) addition without active $N_{2(g)}$ purging.

At the end of electrolysis, the suspension was immediately transferred to an anaerobic chamber, where it was filtered using 0.22 μm filters. The separated solution was reserved for measurements of total dissolved arsenic by flow injection hydride generation atomic absorption spectrometry (FI-HG-AAS) using a PerkinElmer AAnalyst 800. A detailed description of the FI-HG-AAS measurements is presented in the Supplementary Data. The separated solids were used for characterization by XAS. Filtered solids from selected experiments were also characterized by X-ray diffraction (XRD). The XRD data are presented in the Supplementary Data. Finally, a series of chemical extractions using NaOH and phosphate were performed on the solids from a subset of samples to investigate the potential for arsenic remobilization (details in the Supplementary Data).

2.2. X-ray absorption spectroscopy

2.2.1. Data collection

Arsenic K-edge XAS data were collected at Beam Line 4-1 of the Stanford Synchrotron Radiation Lightsource (SSRL, Menlo Park,

USA) and the DUBBLE Beam Line (BM-26) of the European Synchrotron Radiation Facility (ESRF, Grenoble, FR). XANES and EXAFS spectra were recorded for the EC samples and a series of reference samples, consisting of As(III) or As(V) adsorbed to presynthesized GR, 2-line ferrihydrite and Mag (details on adsorption experiments in Supplementary Data). Spectra were recorded at liquid nitrogen temperatures (≈80 K) in fluorescence mode to $k = 13.5$ or 14 $Å^{-1}$. An Au(0) foil was used to calibrate the beam to 11,919 eV (maximum of the first derivative). Spectra were aligned, averaged and background was subtracted using SixPack software (Webb, 2005), following standard methods described previously (van Genuchten et al., 2012). The EXAFS spectra were extracted using k^3-weighting and were Fourier transformed over the *k*-range from 3 to 12 or 13 $Å^{-1}$, using a Kaiser-Bessel window with dk of 3 $Å^{-1}$.

2.2.2. Data analysis

The percentage of As(III) and As(V) sorbed by EC samples was quantified by linear combination fits (LCFs) of the As K-edge XANES spectra, using the SixPack software (Webb, 2005). The reference spectra for As(III) and As(V) adsorbed to GR, 2-line ferrihydrite and Mag were used in the LCFs. The coordination environment of arsenic taken up by the EC samples and the reference materials was determined from shell-by-shell fits using the SixPack software (Webb, 2005). The fits were performed from 1 to 3.5 Å in R+ΔR-space using algorithms derived from IFEFFIT (Newville, 2001). Parameters varied in the fits typically included the interatomic distance (R), the coordination number (CN), the mean squared atomic displacement parameter (σ^2) and the change in threshold energy (ΔE_0). Theoretical phase and amplitude functions for single and multiple scattering paths were calculated using FEFF6 (Rehr et al., 1992) and included As–O, As–O–O and As–Fe paths derived from the structure of scorodite ($FeAsO_4 \cdot 2H_2O$) (Kitahama et al., 1975). The goodness-of-fit was assessed using the R-factor, which is the mean square difference between the fit and the data on a point-by-point basis: $R = \sum_i(data_i - fit_i)^2 / \sum_i(data_i)^2$. A reasonable fit is considered to yield an R-factor less than 0.05 (Kelly et al., 2008). Further details regarding the collection and analysis of XAS data are reported in the Supplementary Data.

3. Results and discussion

3.1. Formation of Fe (hydr)oxide precipitates during Fe(0) EC

Introduction of Fe(II) by Fe(0) electrolysis consumed dissolved oxygen (O_2) and resulted in the formation of insoluble Fe (hydr) oxides in the presence of dissolved arsenic. The production of the various Fe phases, including GR, Fe(III) precipitates, and Mag, depended on key (electro)chemical variables. In experiments to generate GR, the high rate of Fe(II) addition (300 μM Fe(II)/min) was greater than the rate of O_2 influx from the atmosphere, leading to rapid (<5 min) O_2 depletion. During electrolysis, the solution turned from beige, indicative of Fe(II) oxidation and Fe(III) precipitation, to dark blue-green, indicative of GR (Fig. S1 provides macroscopic images of the suspension). The XRD of EC-generated green rust (EC-GR) formed in the presence and absence of arsenic showed the characteristic Bragg peaks of carbonate GR (Fig. S2), including the intense (003) and (006) reflections near 12° and 24° (2θ). The presence of arsenic during EC-GR formation did not shift XRD peak positions, but peaks were broadened, suggesting decreased crystallinity.

The formation of Fe(III) precipitates by Fe(0) EC required a lower iron(II) production rate of 30 μM Fe(II)/min, and a longer electrolysis time of 100 min, which did not deplete O_2 during electrolysis, resulting in complete Fe(II) oxidation. XRD patterns of the orange solids showed peaks for lepidocrocite and broad peaks of poorly ordered Fe(III) (oxyhydr)oxides. The contribution of broad peaks increased in the presence of arsenic, suggesting that arsenic decreased the crystallinity of the ferric precipitates. Because XRD showed evidence for both lepidocrocite and poorly ordered Fe(III) precipitates, we refer henceforth to these samples as ferric (oxyhydr)oxides (Fe(III) oxides).

Similar to the EC-GR experiments, the formation of Mag by Fe(0) EC required an Fe(II) production rate of 300 μM Fe(II)/min applied for 10 min, which depleted O_2, leaving Fe(II) available for mineral formation. Peaks in the XRD patterns of the black solids (Figs. S1 and S2) generated in the presence and absence of arsenic were consistent with magnetite, including the main (220), (400) and (440) peaks at ~30°, ~43° and ~63° 2θ. The major peaks were shifted slightly to higher angle in the presence of arsenic and were also broadened, especially at As/Fe solid ratios >1 mol%.

3.2. Arsenic removal as a function of pH and Fe phase

The concentration of residual aqueous arsenic depended on a number of factors, including the initial concentration of As(V) or As(III), the pH and the type of Fe phase produced (Fig. 1). When EC-GR formed, approximately 98–99% removal of arsenic that had been added as As(V) was achieved, with more effective removal at pH 7.5 than pH 9. EC-GR decreased the As(V) concentration to <10 μg/L for initial As(V) ≤2200 μg/L at pH 7.5 and < 1100 μg/L at pH 9. However, EC-GR could not meet the 1 μg/L target for any initial As(V) concentration or pH. When EC-GR was formed with As(III), the residual arsenic concentration was higher, which is consistent with the lower sorption affinity of As(III) for Fe (hydr)oxides than As(V) in the investigated pH range (Roberts et al., 2004). Approximately 67–84% of initial As(III) was removed at pH 7.5, with the percentage increasing with decreasing initial As(III) concentration (Fig. 1B). Arsenite removal by EC-GR was slightly more effective at pH 9 (78–87%) than 7.5, in contrast to removal of As(V). The residual arsenic level exceeded the 10 μg/L WHO provisional limit for all EC-GR experiments in As(III) solutions.

When Fe(III) oxides formed by EC, both As(V) and As(III) were more effectively removed than with EC-GR. At pH 7.5, EC-Fe(III) oxides removed >99.9% of all initial As(V); only the experiment with the highest initial As(V) concentration had residual arsenic >1 μg/L. Removal of As(V) by Fe(III) oxides was also effective at pH 9 (>99.9% for each sample), but no experiment that produced Fe(III) oxides at pH 9 achieved the 1 μg/L target. The enhanced removal over EC-GR was most pronounced for experiments in As(III) solutions. At pH 7.5, EC-Fe(III) oxides removed more than 99% of the initial As(III) at all tested concentrations, decreasing residual arsenic to near 1 μg/L for some samples and below 10 μg/L for all but the highest initial As(III) concentration (11,000 μg/L, As/Fe = 5 mol%). Arsenite removal by EC-Fe(III) oxides was less effective at pH 9 than 7.5, leading to residual arsenic concentrations near 10 μg/L at pH 9 (Fig. 1).

Although arsenic removal was effective with Fe(III) oxides and GR formed by EC, EC-Mag outperformed both. In all experiments with initial As(V) (220–7000 μg/L) at both pH 7.5 and 9, EC-Mag achieved >99.9% removal and decreased the residual arsenic level to <1 μg/L. This outstanding As(V) removal easily satisfies the WHO 10 μg/L limit and also meets the 1 μg/L target. The removal of As(III) by EC-Mag was also superior, with >99.9% removal of each initial As(III) concentration, regardless of pH. At both pH 7.5 and 9, residual arsenic was <1 μg/L for initial As(III) ≤1100 μg/L.

3.3. Arsenic oxidation state by As K-edge XANES analysis

For EC-GR formed with As(V), the XANES spectra had a smooth absorption edge, with a maximum near 11,875 eV, matching the

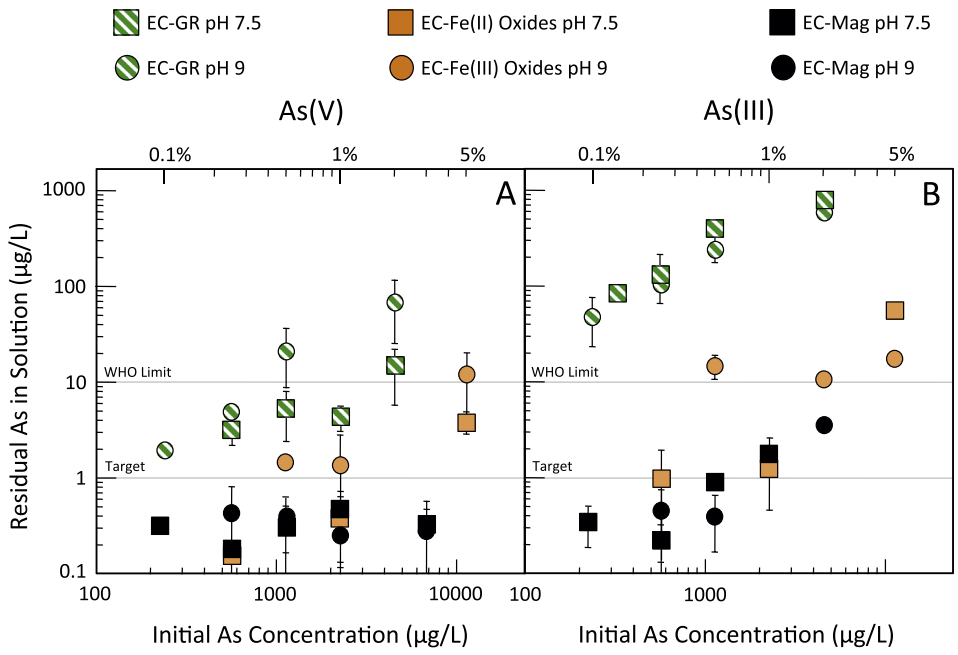

Fig. 1. Aqueous arsenic concentration at the end of the EC experiment, as a function of the initial arsenic concentration (bottom axis) and As/Fe mol% (top axis) for As(V) (Panel A) and As(III) experiments (Panel B). The green, orange and black symbols represent EC-green rust, EC-Fe(III) oxides and EC-magnetite at pH 7.5 (squares) and pH 9 (circles). Error bars represent the standard deviation of replicate measurements; some error bars are smaller than the symbols. (For interpretation of the references to colour in this figure legend, the reader is referred to the Web version of this article.)

peak position from the reference spectrum of As(V) adsorbed to GR (Fig. 2A). The absence of a shoulder at lower energy indicates that significant As(V) reduction did not occur, consistent with the negligible As(III) fraction determined in the XANES LCFs (Table S1). For EC-GR formed with As(III), the distinct shoulders in the XANES spectra indicate that As(III) was partially oxidized. At initial concentrations of 2200 µg/L As(III) (1 mol% As/Fe), the fractions of As(III) (68%) and As(V) (33%) sorbed by EC-GR were similar at both pH 7.5 and 9 (Table S1).

Arsenic sorbed by EC-Fe(III) oxides was present almost exclusively as As(V), regardless of initial As(V) or As(III) concentrations and pH (Fig. 2B, Table S1). Consistent with the EC-GR system, the XANES spectra showed no evidence for the reduction of As(V). For EC-Fe(III) oxides generated in 2200 µg/L As(III) (1 mol% As/Fe) at pH 7.5, the XANES LCFs indicated that arsenic was bound primarily as As(V) (97%). This fraction is substantially higher than the 33% As(V) bound to EC-GR produced at equivalent As(III) concentrations and pH. At the highest initial As(III) concentration (11,000 µg/L, 5 mol% As/Fe) and pH 7.5, which are conditions that should favor the lowest fraction of As(III) oxidation (Li et al., 2012; van Genuchten et al., 2012), As(V) was still the predominant species (86%) detected by XANES LCFs.

The XANES-derived oxidation states of arsenic taken up by EC-Mag matched those of EC-GR samples (Fig. 2C, Table S1). While it has been proposed that As(V) uptake by magnetite can produce small fractions of As(III) (Huhmann et al., 2017), the XANES LCFs did not support the presence of reduced arsenic in EC-Mag samples (Table S1). For EC-Mag formed with As(III), the oxidation to As(V) was effective (70%) at pH 7.5 and initial As(III) = 220 µg/L (0.1 mol% As/Fe). However, at the same pH, the fraction of As(V) bound to EC-Mag decreased to 13% for initial As(III) concentrations of 1100 µg/L (0.5 mol% As/Fe). The significantly greater uptake of arsenic by EC-Mag relative to EC-GR, but similar fractions of surface-bound As(III) and As(V), suggests that the enhanced arsenic removal by EC-Mag is caused by processes beyond As(III) oxidation.

Although the positions of the As(III) and As(V) shoulders in the absorption edge of the EC-Mag samples match those of the As(III) and As(V) adsorption references (Fig. 2C), unique post edge features are present in EC-Mag samples. These oscillations, which have maxima near 11,880 and 11,892 eV, appear in EC-Mag formed with both As(III) or As(V), but are absent from all other EC samples and the adsorption references. These distinct post edge oscillations, which have also been observed in the As K-edge XANES spectra of magnetite produced by biogenic Fe(III) reduction in the presence of As(III) or As(V) (Wang et al., 2014), hints at a different coordination environment of arsenic taken up by EC-Mag relative to the other EC samples.

3.4. Arsenic coordination environment by As K-edge EXAFS analysis

Comparison of EXAFS spectra. The EXAFS spectra of EC-GR generated in As(V) solutions (Fig. 2D) are characterized by smooth, symmetric oscillations, with the exception of the peak near 5 $Å^{-1}$. This asymmetric peak contains a shoulder at lower k, which is more pronounced in the reference EXAFS spectrum of As(V) adsorbed to GR. Little difference in the EXAFS spectra of EC-GR formed with As(V) at increasing As/Fe loading was observed. For EC-GR produced in As(III) solutions, the EXAFS spectra have lower amplitude than As(V) samples, with flatter, more plateaued oscillations near 5 and 7 $Å^{-1}$. Compared with the As(III) and As(V) GR adsorption references, the flattened oscillations in the EC-GR As(III) samples likely arise from the combination of EXAFS signals from sorbed As(III) and As(V), consistent with the XANES analysis.

The EXAFS spectra of EC-Fe(III) oxides generated in the presence of As(V) were similar to those for EC-GR (Fig. 2E), including the asymmetric peak near 5 $Å^{-1}$ and the smooth oscillations at $k > 5$ $Å^{-1}$. The EXAFS spectra of the As(III) EC-Fe(III) oxide samples matched well with those generated in As(V) solutions, in agreement with the predominance of As(V) determined in the XANES LCFs. Regardless of the initial arsenic oxidation state, the EXAFS spectra of EC-Fe(III) oxides strongly resembled the reference spectrum of As(V) adsorbed to ferrihydrite.

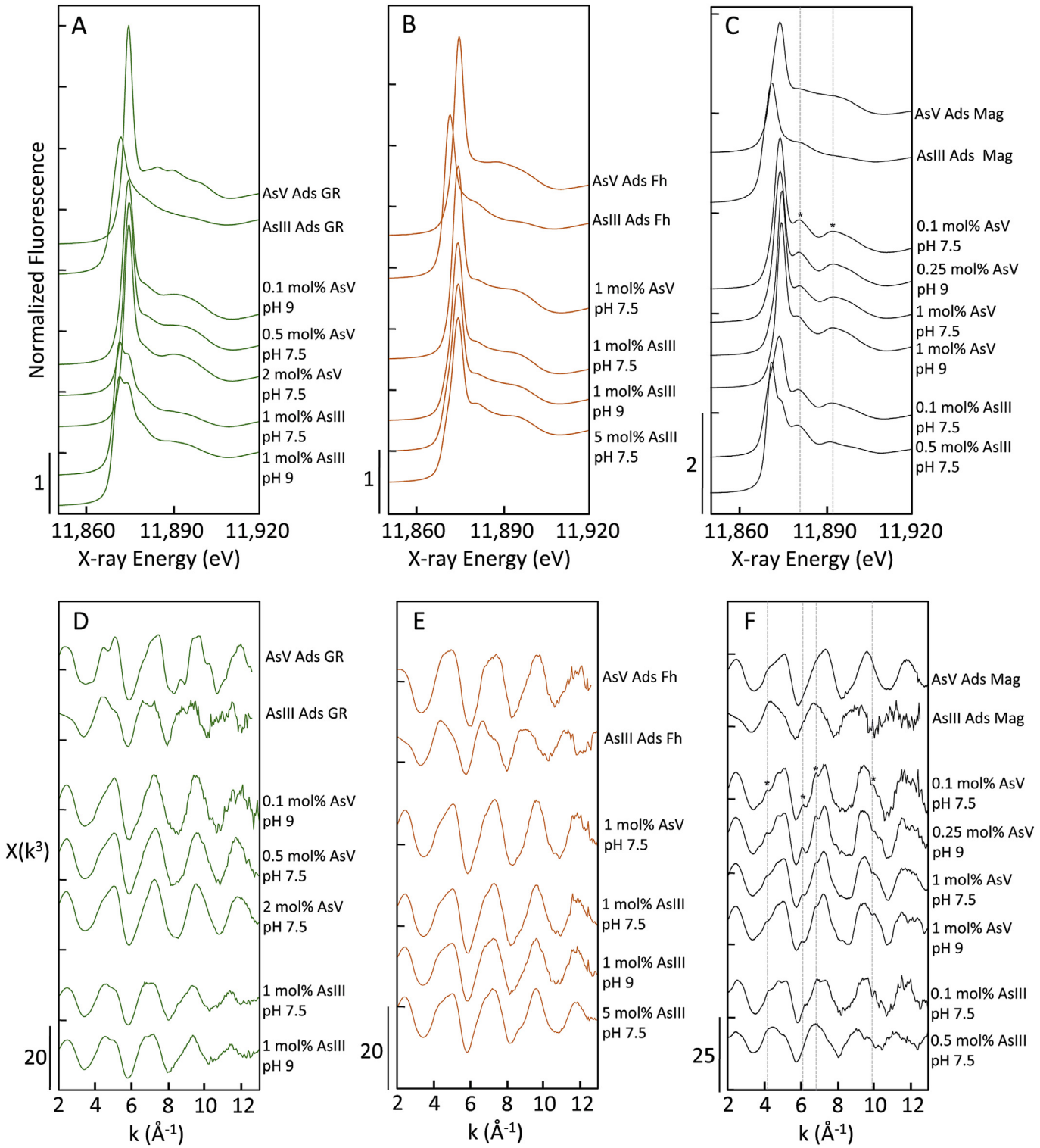

Fig. 2. Arsenic K-edge X-ray absorption near edge structure (XANES) spectra (A-C) and extended X-ray absorption fine structure (EXAFS) spectra (D-F) for EC-green rust (left panels), EC-Fe(III) oxides (middle panels) and EC-magnetite (right panels). As(III) and As(V) adsorption standards are also provided. The vertical grey lines and * highlight features in the XANES and EXAFS spectra of EC-magnetite samples that suggest a different arsenic uptake mode relative to the other EC samples. (For interpretation of the references to colour in this figure legend, the reader is referred to the Web version of this article.)

In contrast to the smooth oscillations of the EC-GR and EC-Fe(III) oxides EXAFS spectra, pronounced beat features permeated the EC-Mag EXAFS spectra (Fig. 2F). In particular, distinct bumps at 4.1 and 6.9 $Å^{-1}$ appeared in the first major EXAFS oscillations. A shoulder at higher k was also present in the oscillation at 9.5 $Å^{-1}$, which contrasts the symmetric shape of this oscillation in the other EC samples. These features were present in all EC-Mag samples generated with As(V) and were also evident for EC-Mag formed

with 220 μg/L As(III). Combined with the unique post edge oscillations in the XANES spectra, the additional beat features in the EC-Mag EXAFS spectra further imply a different arsenic coordination environment than for EC-GR and EC-Fe(III) oxides and the As(III) and As(V) adsorption references.

Shell-by-shell fits of the Fourier transformed EXAFS spectra. For EC-GR produced in As(V) solutions, the shell-by-shell fits resulted in similar first shell As–O parameters, with coordination numbers (CN) ranging from 3.7 to 4.0 and interatomic distances (R) of 1.70 Å (Fig. 3A, Table 1, Table S2). These values are in good agreement with those from fits of the reference spectrum of As(V) adsorbed to GR and are consistent with As–O scattering from As(V) tetrahedra (Waychunas et al., 1993). Fits of the second-shell peak, which arises from As–Fe atomic pairs, were also similar for all EC-GR samples formed with As(V), regardless of pH and solids ratio (0.1–2 mol% As/Fe). Fits of the second-shell peak for these samples yielded $CN_{As\text{-}Fe} = 1.9$ to 2.0 and $R_{As\text{-}Fe} = 3.40$ to 3.43 Å. Compared to the fit of the reference spectrum of As(V) adsorbed to GR

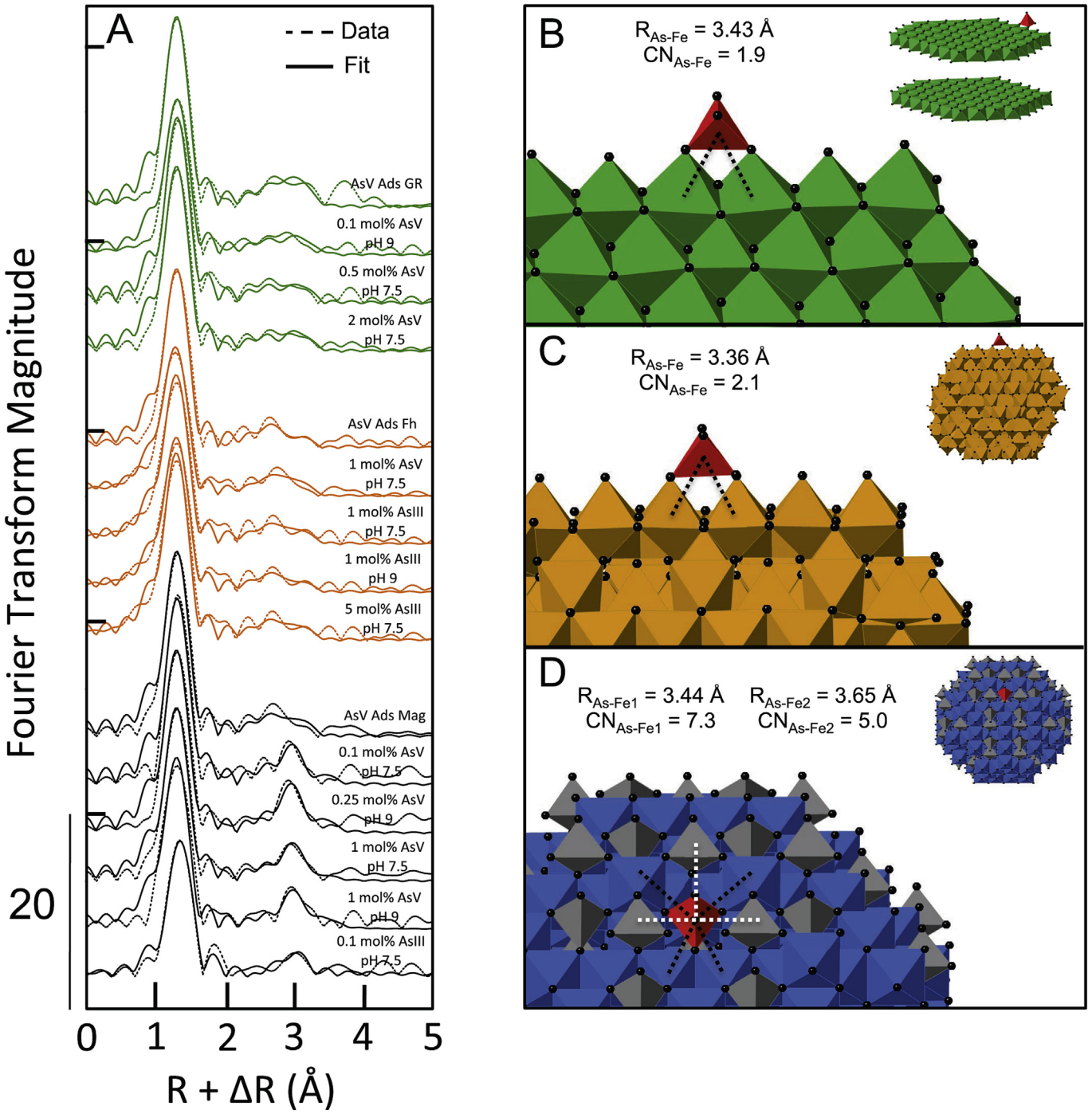

Fig. 3. Fourier-transformed EXAFS spectra of selected EC samples and adsorption references (A) and arsenic uptake models derived by shell-by-shell fits (B-D). The $CN_{As\text{-}Fe}$ and $R_{As\text{-}Fe}$ values given in panels B-D were selected from the fits of individual EC-GR, EC-Fe(III) oxides and EC-Mag samples. The fit-derived errors on the fits appear in Table 1. The broken lines in B, C and D highlight As–Fe atomic pairs.

Table 1
Summary of shell-by-shell fitting results for selected EC samples and adsorption reference materials.

Sample	Atomic Pairs	CN	R (Å)	σ^2 (Å^2)	ΔE_0 (eV)	R-Factor
Green Rust Adsorbed As(V)	As—O	4.0 (0.4)	1.69 (0.01)	0.002 (0.001)	7.2 (1.6)	0.027
	As—O—O	12	1.82(R_{As-O}) = 3.08	σ^2 (As—O)		
	As—Fe1	3.1 (0.9)	3.38 (0.02)	0.009		
EC Green Rust	As—O	3.8 (0.5)	1.70 (0.01)	0.003 (0.001)	8.5 (1.8)	0.041
0.1 mol% As(V) pH 9	As—O—O	12	1.82(R_{As-O}) = 3.10	σ^2 (As—O)		
	As—Fe1	1.9 (1.0)	3.43 (0.03)	0.009		
EC Green Rust	As—O	4.0 (0.4)	1.70 (0.01)	0.002 (0.001)	7.2 (1.5)	0.023
2 mol% As(V) pH 7.5	As—O—O	12	1.82(R_{As-O}) = 3.09	σ^2 (As—O)		
	As—Fe1	2.0 (0.8)	3.41 (0.03)	0.009		
2-Line Ferrihydrite Adsorbed As(V)	As—O	4.1 (0.5)	1.70 (0.01)	0.003 (0.001)	8.0 (1.8)	0.035
	As—O—O	12	1.82(R_{As-O}) = 3.09	σ^2 (As—O)		
	As—Fe1	1.8 (1.0)	3.29 (0.04)	0.010		
EC Fe(III) oxides	As—O	4.6 (0.5)	1.70 (0.01)	0.003 (0.001)	6.8 (1.5)	0.024
1 mol% As(V) pH 7.5	As—O—O	12	1.82(R_{As-O}) = 3.09	σ^2 (As—O)		
	As—Fe1	2.1 (0.9)	3.36 (0.03)	0.010		
EC Fe(III) oxides	As—O	4.4 (0.5)	1.70 (0.01)	0.003 (0.001)	6.3 (1.6)	0.026
1 mol% As(III) pH 7.5	As—O—O	12	1.82(R_{As-O}) = 3.09	σ^2 (As—O)		
	As—Fe1	2.1 (0.9)	3.36 (0.03)	0.010		
Magnetite	As—O	3.9 (0.4)	1.70 (0.01)	0.002 (0.001)	8.0 (1.4)	0.028
Adsorbed As(V)	As—O—O	12	1.82(R_{As-O}) = 3.09	σ^2 (As—O)		
	As—Fe1	2.1 (0.8)	3.36 (0.02)	0.009		
EC Magnetite	As—O	3.9 (0.5)	1.70 (0.01)	0.002 (0.001)	6.0 (1.7)	0.036
0.25 mol% As(V) pH 9	As—O—O	12	1.82(R_{As-O}) = 3.09	σ^2 (As—O)		
	As—Fe1	7.3 (1.8)	3.44 (0.02)	0.009		
	As—Fe2	5.0 (2.1)	3.65 (0.02)	σ^2 (As—Fe1)		
EC Magnetite	As—O	2.9 (0.4)	1.72 (0.01)	0.001 (0.001)	11.6 (1.7)	0.030
0.1 mol% As(III) pH 7.5	As—O—O	12	1.82(R_{As-O}) = 3.12	σ^2 (As—O)		
	As—Fe1	2.4 (1.4)	3.42 (0.04)	0.009		
	As—Fe2	1.2 (1.7)	3.61 (0.09)	σ^2 (As—Fe1)		

CN represents the coordination number, R, the interatomic distance, σ^2, the mean squared atomic displacement and ΔE_0, the change in threshold energy. The passive electron reduction factor, S_0^2, was fixed at 1.0. Fitting parameters allowed to float are accompanied by fit-determined standard errors in parenthesis, whereas constrained parameters are written without parentheses. The distance of multiple scattering from As—O—O (CN = 12 for As(V)) was constrained geometrically to the single scattering As—O path ($R_{As-O-O} = 1.82\ R_{As-O}$). All fits were carried out from 1 to 3.5 Å in R+ΔR-space. Fits for the rest of the samples are presented in Table S2.

($CN_{As-Fe} = 3.1 \pm 0.9$, $R_{As-Fe} = 3.38 \pm 0.02$ Å), EC-GR had a slightly lower second-shell CN and longer R.

The fitting output for the first and second shell peaks of EC-Fe(III) oxides were similar, regardless of pH and the concentration and initial oxidation state of arsenic. The first shell was fit with an As—O path with $CN_{As-O} = 4.1$ to 4.6 and $R_{As-O} = 1.70$ Å (Table 1, Table S2). The second shell was fit with an As—Fe path with $CN_{As-Fe} = 1.7$ to 2.3 and $R_{As-Fe} = 3.34$ to 3.36 Å. These fitting parameters matched well with those from the fit of As(V) adsorbed to ferrihydrite ($CN_{As-O} = 4.1 \pm 0.5$, $R_{As-O} = 1.70 \pm 0.1$ Å, $CN_{As-Fe} = 1.8 \pm 1.0$ and R_{As-Fe} 3.29 ± 0.02 Å). However, the second shell R_{As-Fe} for EC-Fe(III) oxides was slightly longer than for the ferrihydrite adsorption reference, which reflects the presence of both lepidocrocite and ferrihydrite in EC-Fe(III) oxides, consistent with the XRD.

The fits of the first As—O shell of EC-Mag samples generated with As(V) were similar to those for EC-GR and EC-Fe(III) oxides, yielding $CN_{As-O} = 3.6$ to 3.9 and $R_{As-Fe} = 1.70$ Å (Table 1, Table S2). However, in contrast to the second shell fits for EC-GR and EC-Fe(III) oxides spectra, which required only a single As—Fe path, the fit of the EC-Mag spectra required two As—Fe paths. The parameters returned by the fit for the first As—Fe path were $CN_{As-Fe1} = 5.1$ to 7.3 and $R_{As-Fe1} = 3.44$ to 3.47 Å, whereas the second As—Fe path had $CN_{As-Fe2} = 2.8$ to 5.0 and $R_{As-Fe2} = 3.64$ to 3.68 Å. These CN and R values are significantly different than those obtained in fits of the reference spectrum for As(V) adsorbed to presynthesized Mag ($CN_{As-Fe} = 2.1 \pm 0.8$, $R_{As-Fe} = 3.36 \pm 0.02$ Å) and also differ from the EC-GR and EC-Fe(III) oxides spectra. This indicates a different arsenic uptake mode by EC-Mag.

Multiple As—Fe atomic pairs at different spacing were also required in the fit of the spectrum for EC-Mag generated in 220 μg/L As(III). For this sample, the first shell was fit with $CN_{As-O} = 2.9 \pm 0.4$ and $R_{As-O} = 1.72 \pm 0.1$ Å. This fit-derived R_{As-O} is consistent with the presence of both As(III) and As(V) determined from the XANES LCFs. The second shell of this sample was fit using As—Fe atomic pairs at $R_{As-Fe1} = 3.42 \pm 0.04$ Å and $R_{As-Fe2} = 3.61 \pm 0.09$ (Table 1). Although the fit-derived CN for these As—Fe paths was <3, the comparable R_{As-Fe1} and R_{As-Fe2} for this sample and the As(V) samples in the EC-Mag system was strong evidence for similar arsenic sorption configurations.

3.5. Modes of arsenic uptake by EC-GR, EC-Fe(III) oxides and EC-Mag

The shell-by-shell fits indicate that arsenic binds to both EC-GR and EC-Fe(III) oxides primarily in the binuclear, corner sharing (^{2}C) surface complex (Fig. 3). This conclusion is founded on the fit-derived $CN_{As-Fe} = 1.9$ to 2.0 and $R_{As-Fe} = 3.40$ to 3.43 Å for EC-GR spectra and $CN_{As-Fe} = 1.7$ to 2.3 and $R_{As-Fe} = 3.34$ to 3.36 Å for EC-Fe(III) oxides spectra (Table 1, Table S2). The fitting output is in excellent agreement with previous EXAFS studies of As(V) adsorbed to GR-CO_3 (Jonsson and Sherman, 2008) and Fe(III) oxides (Waychunas et al., 1993) and is inconsistent with the formation of distinct As-bearing Fe(II) (parasymplesite) (Babechuk et al., 2009) or Fe(III) (scorodite) (Kitahama et al., 1975) minerals. The formation of similar binuclear, corner sharing ^{2}C adsorption geometries for

EC-GR and EC-Fe(III) oxides is supported by the match between the shorter $R_{As\text{-}Fe}$ for EC-Fe(III) oxides (3.34–3.36 Å) than for EC-GR spectra (3.40–3.43 Å) and the shorter average $R_{Fe\text{-}O}$ (2.01 Å) and $R_{Fe\text{-}Fe}$ (3.05 Å) for edge sharing FeO_6 octahedra in Fe(III) (oxyhydr) oxides (Wyckoff, 1963) relative to GR ($R_{Fe\text{-}O} = 2.08$ Å, $R_{Fe\text{-}Fe} = 3.18$ Å) (Trolard et al., 2007). Although layered double hydroxides, such as GR, can take up oxyanions as outer sphere complexes in the interlayer (Ma et al. 2017, 2018), our data do not support this arsenic uptake mode, which would lack the observed As–Fe atomic pair and, most likely, change the spacing for the basal plane reflections in XRD. Therefore, arsenic adsorption to EC-GR particle edges and EC-Fe(III) oxide surfaces is the most likely uptake mode for these samples.

In contrast to the fits of EC-GR and EC-Fe(III) oxides, the fits for EC-Mag required two sets of As–Fe atomic pairs at 3.42 to 3.47 Å and 3.61 to 3.68 Å, consistent with arsenic occupying tetrahedral FeO_4 sites in the magnetite structure (Wang et al., 2011). Based on the magnetite crystal structure (Bragg, 1915), arsenic substitution for Fe in tetrahedral coordination would result in theoretical $R_{As\text{-}Fe1}$ and $R_{As\text{-}Fe2} = 3.45$ Å and 3.60 Å, which correspond to arsenic bonding with nearest neighbor FeO_6 octahedra and nearest neighbor FeO_4 tetrahedra (Fig. 3D). These theoretical $R_{As\text{-}Fe}$ values are in excellent agreement with the fit-derived values. However, the fit-derived $CN_{As\text{-}Fe}$ for EC-Mag samples are lower ($CN_{As\text{-}Fe1} < 7.3$, Table 1, Table S2) than the theoretical CN of arsenic incorporated perfectly into bulk magnetite ($CN_{As\text{-}Fe1,Inc} = 12$). Two scenarios can explain this: i) the co-existence of adsorbed and completely incorporated arsenic and ii) the substitution of arsenic for tetrahedral FeO_4 near the surface of the EC-Mag particle, i.e. partial incorporation. We argue against the first explanation for several reasons. First, chemical extractions with NaOH and phosphate that target adsorbed arsenic only mobilized 12 and 4% of arsenic taken up by EC-Mag, which was significantly less than the 38 and 33% mobilized from ferrihydrite (Fig. S3). Shell-by-shell fits of the extracted and initial EC-Mag samples yielded similar $CN_{As\text{-}Fe}$ values (within fit-derived error), which is inconsistent with the mobilization of strictly adsorbed arsenic (Table S3). Second, extensive incorporation of arsenic in the bulk structure is unlikely because of differences in the charge and size of FeO_4 (Fe^{3+}, $R_{Fe\text{-}O} = 1.80$ Å) and AsO_4 (As^{5+}, $R_{As\text{-}O} = 1.70$ Å) (Wang et al., 2011), which would generate strain and require charge compensation, most likely in the form of Fe vacancies. Partial incorporation of arsenic at the outermost part of the particle would be accommodated more easily because of structural relaxation at the surface and easier balancing of charge by surface deprotonation. Finally, the nanoscale particle size of EC-Mag, i.e. <5 nm diameter crystallites (van Genuchten et al., 2018), gives rise to a high ratio of surface to bulk, which facilitates partial arsenic incorporation at the particle exterior. Therefore, we propose that arsenic removal occurs by occupation of tetrahedral FeO_4 sites near the surface of EC-Mag (Fig. 3D). Several possible sorption configurations consistent with our data are presented in Fig. S4. Incomplete As(III) oxidation in the EC-Mag system produces a mixture of partially incorporated As(V) and adsorbed As(III), but from our data, partial As(III) incorporation cannot be ruled out.

3.6. Factors influencing residual arsenic during Fe (hydr)oxide formation by EC

For experiments in both As(III) and As(V) solutions, the residual arsenic concentration decreased in order of EC-GR > EC-Fe(III) oxides > EC-Mag, with EC-Mag achieving <1 μg/L arsenic in all but the highest As(III) experiments. Furthermore, the ratio of arsenic partitioning to the solid (μg/g) and liquid (μg/L) phase for the three types of Fe (oxyhydr)oxides increased in the same order: EC-GR = 21.6 L/g, EC-Fe(III) oxides = 466 L/g, EC-Mag = 16,800 L/g for experiments with 1125 μg/L (15 μM) initial As(III) at pH 9. These trends in removal efficiency and affinity for the solid phase can be explained by synthesis conditions, structural properties of the solids and differences in the As(III) and As(V) sorption affinity for Fe (hydr)oxide surfaces. The modes of arsenic uptake by EC-GR and EC-Fe(III) oxides were similar (i.e. binuclear ^{2}C adsorption geometry, Fig. 3), which indicates the more effective removal of arsenic by EC-Fe(III) oxides is not a result of the arsenic coordination geometry. The XANES analysis revealed a lower extent of As(III) oxidation during formation of EC-GR than EC-Fe(III) oxides, which is due to the higher Fe(II) production rate during EC-GR experiments. The build up of Fe(II) at high Fe(II) production rates is required for GR formation, but Fe(II) also competes with As(III) for the Fenton-type oxidants ($^*O_2^-$, Fe(IV)) generated in EC systems (Li et al., 2012; van Genuchten et al., 2012). Less competition between Fe(II) and As(III) for reactive oxidants occurs at the low Fe(II) production rate required for EC-Fe(III) oxide formation (van Genuchten et al., 2018), which leads to more effective generation of the readily adsorbed As(V) oxyanion and lower residual arsenic concentration (Roberts et al., 2004). In As(V) solutions, the differences between arsenic removal by EC-GR and EC-Fe(III) oxides were less pronounced than in As(III) solutions. Although carbonate competes weakly with arsenic for Fe (hydr)oxide surfaces (Brechbuhl et al., 2012; Meng et al., 2000), the more effective removal of As(V) by EC-Fe(III) oxides than EC-GR is best explained by differences in the density and type of reactive sorption sites. Poorly crystalline Fe(III) precipitates (Spadini et al., 2003) are expected to have higher specific surface and more diverse surface structure than moderately crystalline GR (Williams and Scherer, 2001), which has an ordered sheet structure with arsenic sorption sites located primarily on particle edges (Wang et al., 2010).

Concomitant with the best arsenic removal performance (Fig. 1), the spectra from EC-Mag also displayed XANES and EXAFS features consistent with a unique arsenic uptake mode where arsenic substitutes for FeO_4 tetrahedra near the particle surface. This sorption configuration was detected in EC-Mag produced in both As(V) and As(III) solutions. Arsenic was removed reliably to <1 μg/L when partially incorporated arsenic was detected, and in this sorption mode, arsenic was mobilized less by NaOH and phosphate than when present in the ^{2}C surface complex (Fig. S3). The presence of FeO_4 tetrahedra is the most likely reason partial arsenic incorporation is favorable in EC-Mag, and not in the other EC samples, and this unique arsenic uptake mode explains why EC-Mag bonds arsenic more easily and removes arsenic more effectively. Finally, the efficiency of arsenic removal by EC-Mag was not impacted significantly by pH, whereas As(V) removal by EC-GR and EC-Fe(III) oxides decreased with increasing pH. This likely reflects a transition from net positive to net negative surface charge for GR (Guilbaud et al., 2013) and Fe(III) oxides (Spadini et al., 2003) as pH increases from 7.5 to 9, leading to less favorable sorption of the As(V) oxyanion at pH 9 because of electrostatic repulsion. In contrast, formation of solid solutions (partial incorporation of arsenic in EC-Mag) is less likely to depend on pH.

3.7. Practical considerations for achieving <1 μg/L residual arsenic with EC-Mag

Treatment of drinking water to low levels (<1 μg/L) of arsenic can reduce the disease burden caused by chronic arsenic exposure in high (van Halem et al., 2009) and low income countries (Howard et al., 2007). The Netherlands is currently the only country in the world where the drinking water sector targets 1 μg/L, which arose from comparing the costs of arsenic-related health impacts and water treatment infrastructure (Ahmad and Bhattacharya, 2019;

van der Wens et al., 2016; Ahmad et al., 2019). However, the development of innovative technologies that can achieve 1 μg/L, without major infrastructure renovation, can improve this cost benefit analysis to favor lower arsenic targets, particularly in countries where improvements to treatment infrastructure are prohibitively costly. In this study, we have shown that formation of Mag by Fe(0) electrolysis reliably yields residual arsenic <1 μg/L for a wide range of initial conditions, whereas EC-Fe(III) oxides and EC-GR would require more charge passed (i.e. more electricity and Fe consumed and thus more costs) to meet 1 μg/L, if possible at all. Arsenic removal to <1 μg/L is difficult to achieve using other treatment methods, such as $FeCl_3$ addition without As(III) preoxidation (Hering et al., 1996), passive Fe(0) corrosion (Leupin et al., 2005; Neumann et al., 2013) and membrane techniques (Schmidt et al., 2016). In some cases, removal to <1 μg/L has been reported using adsorption media that require sophisticated synthesis procedures and costly materials (Chandra et al., 2010; Luo et al., 2012) or by augmenting conventional $FeCl_3$ addition by preoxidation with $KMnO_4$ (Ahmad et al., 2018). However, EC-Mag formation is a promising alternative because high concentrations of both As(V) and As(III) can be treated to <1 μg/L at a range of pH (7.5–9) and it requires only a small input of electricity and small amounts of Fe(0) metal, which is readily available everywhere and completely non-hazardous.

Our experiments were designed to compare the arsenic removal efficiency of EC-Mag, EC-GR and EC-Fe(III) oxides using a constant Fe dosage (3 mM total Fe) and systematically varied initial arsenic concentration spanning the range of the worst case scenario geogenic arsenic levels (e.g. BGS, 2001). While we show that EC-Mag outperformed EC-Fe(III) oxides, primarily at arsenic levels >500 μg/L and at pH 9, it is reasonable to expect that EC-Mag would similarly outperform EC-Fe(III) oxides at lower initial arsenic levels if the total Fe dosage is optimized. For example, because 3 mM EC-Mag could remove 1125 μg/L initial As(III) to <1 μg/L at pH 9, which was not possible for EC-Fe(III) oxides (Fig. 1), EC-Mag would likely require significantly less Fe than EC-Fe(III) oxides for full removal of 50 μg/L As(III) at pH 9. Our study sets the foundation for subsequent research to optimize the total EC-Mag concentration required to achieve <1 μg/L for a constant arsenic level, which would help to more accurately identify the best Fe(0) EC operating conditions for field treatment.

Another important practical consideration for arsenic treatment is the appropriate management of arsenic-rich waste that is generated as a by-product from all arsenic removal methods (e.g. $FeCl_3$ addition, membrane filtration, Fe(0) EC). The formation of Mag by Fe(0) EC is more attractive than the production of Fe(III) oxides with respect to waste production for several reasons. As the chemical formula (Fe_3O_4) shows, the mass ratio of Fe to total solid is higher for Mag (0.72) than for Fe(III) oxides (i.e. ferrihydrite, with an approximate chemical formula of $Fe(OH)_3$, has a Fe mass ratio of 0.52). Therefore, per mol of Fe generated by EC, the formation of Mag theoretically produces 28% less sludge mass (3 mM Fe = 232 mg Fe_3O_4/L) than ferrihydrite (3 mM Fe = 321 mg $Fe(OH)_3$/L), the most common Fe(III) precipitate formed in arsenic treatment by $FeCl_3$ addition (Hering et al., 1996). Also, the density of Mag (5.3 g/cm^3) is higher than that of ferrihydrite (3.4 g/cm^3) because it has less space-filling O atoms per Fe atom (1.33 O/Fe for Fe_3O_4, 3 O/Fe for $Fe(OH)_3$). Therefore, per mol of Fe generated by EC, 36% less sludge volume would be generated for Mag than for ferrihydrite. An additional benefit is the ease of separating EC-Mag particles from treated water using low strength magnetic fields, which would likely facilitate sludge dewatering. We also found that arsenic taken up by partial incorporation in the EC-Mag structure is more resistant to mobilization than when associated with ferrihydrite (Fig. S3), making arsenic exposure less likely during EC-Mag sludge handling and storage. Finally, Mag is one of the highest valued Fe oxides, having applications across several industries (e.g. electronics, catalysis, and biotechnology), which makes reuse of Mag treatment sludge more appealing than ferrihydrite (Gawande et al., 2013; Arbab et al., 2003).

With respect to infrastructure requirements, Fe(0) EC systems, and the production of EC-Mag in particular, also offers a number of benefits relative to conventional treatment methods, such as $FeCl_3$ addition. For example, per mass of iron, steel is cheaper (hot rolled plate steel ≈800$ per ton of Fe) (MEPS, 2018) than the 40% $FeCl_3$ solution used in conventional water treatment (≈1450$ per ton of Fe) (Alibaba.com, 2018). Transport of the more dense Fe(0) metal to the treatment site is also easier and cheaper than the large volumes of acidic $FeCl_3$ solution and the treated water does not inherit unnecessary chloride. Although Fe(0) EC systems require electricity, energy consumption is comparable or lower than other methods (e.g. reverse osmosis) (Schmidt et al., 2016) and it can be provided by sustainable power sources, such as photovoltaics and fuel cells. Finally, low cost separation of EC-Mag particles using a magnetic field would eliminating extra requirements for coagulation or filtration to complete treatment (Yavuz et al., 2006).

In summary, our results suggest that the formation of EC-Mag is one of the most attractive methods to achieve <1 μg/L residual arsenic because this method provides i) exceptional arsenic removal efficiency, ii) unique arsenic uptake modes and resistance to arsenic mobilization, iii) lower mass and volume of sludge produced per mol of Fe, iv) magnetic properties that favor particle separation and v) higher valued sludge than production of Fe(III) oxides. These benefits favor the reuse of the treatment waste. However, additional research is necessary before EC-Mag can be implemented in practice. First, groundwater contaminated by geogenic arsenic often contains substantial concentrations of phosphate and silicate, which can alter the structure of co-precipitated Fe oxides (Voegelin et al., 2010; van Genuchten et al., 2014; Senn et al., 2015) and are well known to compete with arsenic for sorption sites (Roberts et al., 2004). Therefore, the effect of phosphate and silicate on the arsenic removal efficiency of EC-Mag needs to be evaluated. Second, the stability and best management practices of the treatment sludge must be determined.

4. Conclusions

For a given Coulomb of charge passed (or mass of Fe produced), EC-Mag was more effective than EC-Fe(III) oxide and EC-GR at achieving <1 μg/L residual arsenic, regardless of the As(V) or As(III) species or pH. The exceptional performance of EC-Mag is attributed in part to the formation of a unique arsenic sorption mode where arsenic substitutes for tetrahedral iron near the Mag particle surface. While EC-Fe(III) oxides and EC-GR removed arsenic effectively (67–99%), the production of these solids by EC would likely require significantly higher charge passed (and Fe added) to meet 1 μg/L, resulting in greater electricity consumption and more solid waste. Therefore, especially in decentralized treatment systems based on Fe(II) addition, such as Fe(0) EC, magnetite formation is desirable relative to other Fe phases for the following reasons: i) enhanced ability to meet 1 μg/L, ii) more stable arsenic bonding mode that resists mobilization more than standard surface complexes, and iii) potential for simplified particle separation from treated water by magnetic separation.

Declaration of competing interest

The authors declare that they have no known competing financial interests or personal relationships that could have appeared to influence the work reported in this paper.

Acknowledgements

We gratefully acknowledge funding provided by the Dutch Organization for Scientific Research in a Veni Grant to CMvG (Project No. 14400). We thank Marcel Ceccato for assistance with FI-HG-AAS measurements. Synchrotron experiments were performed partly at the DUBBLE beamline at the ESRF, Grenoble, France, with assistance from Dipanjan Banerjee. We also thank Ryan Davis and Sharon Bone for technical support during synchrotron data collection at SSRL. Use of SSRL, SLAC National Accelerator Laboratory, was supported by the U.S. Department of Energy, Office of Science, Basic Energy Sciences, under Contract No. DE-AC02-76SF00515.

Appendix A. Supplementary data

Supplementary data to this article can be found online at https://doi.org/10.1016/j.watres.2019.115170.

References

Ahmad, A., Bhattacharya, P., 2019. Arsenic in drinking water: is 10 μg/L a safe limit? Curr. Pollut. Rep. 5 (1), 1–3.
Ahmad, A., Cornelissen, E., van de Wetering, S., van Dijk, T., van Genuchten, C., Bundschuh, J., van der Wal, A., Bhattacharya, P., 2018. Arsenite removal in groundwater treatment plants by sequential Permanganate—Ferric treatment. J. Water Process Eng. 26, 9.
Ahmad, A., van der Wens, P., Baken, K., de Waal, L., Bhattacharya, P., Stuyfzand, P., 2019. Arsenic reduction to <1 μg/L in Dutch drinking water. Environ. Int. In press.
Alibaba.com, 2018. Industrial Grade, Water Treatment 40% Liquid Ferric Chloride Solution. https://www.alibaba.com/showroom/ferric-chloride-fecl3.html.
Amrose, S.E., Bandaru, S.R.S., Delaire, C., van Genuchten, C.M., Dutta, A., DebSarkar, A., Orr, C., Roy, J., Das, A., Gadgil, A.J., 2014. Electro-chemical arsenic remediation: field trials in West Bengal. Sci. Total Environ. 488–489, 539–546.
Amrose, S.E., Burt, Z., Ray, I., 2015. Safe drinking water for low-income regions. Annu. Rev. Environ. Resour. 40 (9), 203–231.
Arbab, A., Bashaw, L., Miller, B., Jordan, E., Lewis, B., Kalish, H., Frank, J., 2003. Characterization of biophysical and metabolic properties of cells labeled with superparamagnetic iron oxide nanoparticles and transfection agent for cellular MR imaging. Radiology 229 (3), 838–846.
Babechuk, M., Weisener, C., Fryer, B., Paktunc, D., Maunders, C., 2009. Microbial reduction of ferrous arsenate: biogeochemical implications for arsenic mobilization. Appl. Geochem. 24 (12), 2332–2341.
Bard, A.J., Faulkner, L.R., 2001. Electrochemical Methods : Fundamentals and Applications. Wiley, New York.
BGS, 2001. Arsenic contamination of groundwater in Bangladesh. British Geological Survey 1–267.
Bragg, W., 1915. The structure of magnetite and the spinels. Nature 95, 561-561.
Brauner, E., Nordsborg, R., Andersen, Z., Tjonneland, A., Loft, S., Raaschou-Nielsen, O., 2014. Long-term exposure to low-level arsenic in drinking water and diabetes incidence: a prospective study of the diet, cancer and health cohort. Environ. Health Perspect. 122 (10), 1059–1065.
Brechbuhl, Y., Christl, I., Elzinga, E., Kretzschmar, R., 2012. Competitive sorption of carbonate and arsenic to hematite: combined ATR-FTIR and batch experiments. J. Colloid Interface Sci. 377, 313–321.
Chandra, V., Park, J., Chun, Y., Lee, J., Hwang, I., Kim, K., 2010. Water-dispersible magnetite-reduced graphene oxide composites for arsenic removal. ACS Nano 4 (7), 3979–3986.
Dixit, S., Hering, J.G., 2003. Comparison of arsenic(V) and arsenic(III) sorption onto iron oxide minerals: implications for arsenic mobility. Environ. Sci. Technol. 37 (18), 4182–4189.
Gawande, M., Branco, P., Varma, R., 2013. Nano-magnetite (Fe_3O_4) as a support for recyclable catalysts in the development of sustainable methodologies. Chem. Soc. Rev. 42 (8), 3371–3393.
Guilbaud, R., White, M., Poulton, S., 2013. Surface charge and growth of sulphate and carbonate green rust in aqueous media. Geochem. Cosmochim. Acta 108, 141–153.
Hering, J.G., Chen, P.Y., Wilkie, J.A., Elimelech, M., Liang, S., 1996. Arsenic removal by ferric chloride. J. AWWA (Am. Water Works Assoc.) 88 (4), 155–167.
Howard, G., Ahmed, M., Teunis, P., Mahmud, S., Davison, A., Deere, D., 2007. Disease burden estimation to support policy decision-making and research prioritization for arsenic mitigation. J. Water Health 5 (1), 67–81.
Hug, S.J., Leupin, O., 2003. Iron-catalyzed oxidation of arsenic(III) by oxygen and by hydrogen peroxide: pH-dependent formation of oxidants in the Fenton reaction. Environ. Sci. Technol. 37 (12), 2734–2742.
Huhmann, B., Neumann, A., Boyanov, M., Kemner, K., Scherer, M., 2017. Emerging investigator series: as(v) in magnetite: incorporation and redistribution. Environ. Sci. Process. Impacts 19 (10), 1208–1219.
Jonsson, J., Sherman, D.M., 2008. Sorption of As(III) and As(V) to siderite, green rust (fougerite) and magnetite: implications for arsenic release in anoxic groundwaters. Chem. Geol. 255 (1–2), 173–181.
Kapaj, S., Peterson, H., Liber, K., Bhattacharya, P., 2006. Human health effects from chronic arsenic poisoning- A review. J. Environ. Sci. Health - Part A Toxic/Hazard. Subst. Environ. Eng. 41 (10), 2399–2428.
Kelly, S.D., Hesterberg, D., Ravel, B., 2008. Analysis of soils and minerals using X-ray absorption spectroscopy. In: Methods of Soil Analysis. Part 5. Mineralogical Methods. SSA Book Series No.5.
Kitahama, K., Kiriyama, R., Baba, Y., 1975. Refinement of crystal-structure of scorodite. Acta Crystallogr. Sect. B Struct. Sci. 322–324.
Kobya, M., Demirbas, E., Ulu, F., 2016. Evaluation of operating parameters with respect to charge loading on the removal efficiency of arsenic from potable water by electrocoagulation. J. Environ. Chem. Eng. 4 (2), 11.
Kumar, P.R., Chaudhari, S., Khilar, K.C., Mahajan, S.P., 2004. Removal of arsenic from water by electrocoagulation. Chemosphere 55 (9), 1245–1252.
Lakshmanan, D., Clifford, D.A., Samanta, G., 2009. Ferrous and ferric ion generation during iron electrocoagulation. Environ. Sci. Technol. 43 (10), 3853–3859.
Leupin, O., Hug, S., Badruzzaman, A., 2005. Arsenic removal from Bangladesh tube well water with filter columns containing zerovalent iron filings and sand. Environ. Sci. Technol. 39 (20), 8032–8037.
Li, L., van Genuchten, C.M., Addy, S.E.A., Yao, J., Gao, N., Gadgil, A.J., 2012. Modeling As(III) oxidation and removal with iron electrocoagulation in groundwater. Environ. Sci. Technol. 46 (21), 12038–12045.
Luo, X., Wang, C., Luo, S., Dong, R., Tu, X., Zeng, G., 2012. Adsorption of as (III) and as (V) from water using magnetite Fe3O4-reduced graphite oxide-MnO2 nanocomposites. Chem. Eng. J. 187, 45–52.
Ma, B., Fernandez-Martinez, A., Grangeon, S., Toumassat, C., Findling, N., Claret, F., Koishi, A., Marty, N., Tisserand, D., Bureau, S., Salas-Colera, E., Elkaim, E., Marini, C., Charlet, L., 2017. Evidence of multiple sorption modes in layered double hydroxides using Mo as structural probe. Environ. Sci. Technol. 51 (10), 5531–5540.
Ma, B., Fernandez-Martinez, A., Grangeon, S., Tournassat, C., Findling, N., Carrero, S., Tisserand, D., Bureau, S., Elkaim, E., Marini, C., Aquilanti, G., Koishi, A., Marty, N., Charlet, L., 2018. Selenite uptake by Ca-Al LDH: a description of intercalated anion coordination geometries. Environ. Sci. Technol. 52 (3), 1624–1632.
Meng, X.G., Bang, S., Korfiatis, G.P., 2000. Effects of silicate, sulfate, and carbonate on arsenic removal by ferric chloride. Water Res. 34 (4), 1255–1261.
MEPS, 2018. World Carbon Steel Prices. http://www.meps.co.uk/World%20Carbon%20Price.htm.
Müller, S., Behrends, T., van Genuchten, C.M., 2019. Sustaining efficient production of aqueous iron during repeated operation of Fe(0)-electrocoagulation. Water Res. 155, 10.
Naujokas, M., Anderson, B., Ahsan, H., Aposhian, H., Graziano, J., Thompson, C., Suk, W., 2013. The broad scope of health effects from chronic arsenic exposure: update on a worldwide public health problem. Environ. Health Perspect. 121 (3), 295–302.
Neumann, A., Kaegi, R., Voegelin, A., Hussam, A., Munir, A., Hug, S., 2013. Arsenic removal with composite iron matrix filters in Bangladesh: a field and laboratory study. Environ. Sci. Technol. 47 (9), 4544–4554.
Newville, M., 2001. IFEFFIT: interactive XAFS analysis and FEFF fitting. J. Synchrotron Radiat. 322–324.
NHMRC, 2011. In: N.R.M.M (Ed.), Australian Drinking Water Guidelines Paper 6 National Water Quality Management Strategy. Council. National Health and Medical Research Council.
Rahman, M., Ng, J., Naidu, R., 2009. Chronic exposure of arsenic via drinking water and its adverse health impacts on humans. Environ. Geochem. Health 31, 189–200.
Rehr, J., Albers, R., Zabinsky, S., 1992. High-order multiple-scattering calculations of X-ray absorption fine structure. Phys. Rev. Lett. 3397–3400.
Roberts, L.C., Hug, S.J., Ruettimann, T., Billah, M., Khan, A.W., Rahman, M.T., 2004. Arsenic removal with iron(II) and iron(III) in waters with high silicate and phosphate concentrations. Environ. Sci. Technol. 38 (1), 307–315.
Roy, J., 2008. Economic benefits of arsenic removal from ground water - a case study from West Bengal, India. Sci. Total Environ. 397 (1–3), 1–12.
SABS, 2001. In: South African Standard Specifications 241: Drinking Water (Edition 5). South African Bureau of Standards, p. 9.
Saint-Jacques, N., Brown, P., Nauta, L., Boxall, J., Parker, L., Dummer, T., 2018. Estimating the risk of bladder and kidney cancer from exposure to low-levels of arsenic in drinking water, Nova Scotia, Canada. Environ. Int. 110, 95–104.
Schmidt, S., Gukelberger, E., Hermann, M., Fiedler, F., Grossmann, B., Hoinkis, J., Ghosh, A., Chatterjee, D., Bundschuh, J., 2016. Pilot study on arsenic removal from groundwater using a small-scale reverse osmosis system -Towards sustainable drinking water production. J. Hazard Mater. 318, 671–678.
Senn, A.-C., Kaegi, R., Hug, S.J., Hering, J.G., Mangold, S., Voegelin, A., 2015. Composition and structure of Fe(III)-precipitates formed by Fe(II) oxidation in water at near-neutral pH: interdependent effects of phosphate, silicate and Ca. Geochem. Cosmochim. Acta 162, 220–246.
Spadini, L., Schindler, P., Charlet, L., Manceau, A., Ragnarsdottir, K., 2003. Hydrous ferric oxide: evaluation of Cd-HFO surface complexation models combining Cd-K EXAFS data, potentiometric titration results, and surface site structures identified from mineralogical knowledge. J. Colloid Interface Sci. 266 (1), 1–18.
Trolard, F., Bourrie, G., Abdelmoula, M., Refait, P., Feder, F., 2007. Fougerite, a new mineral of the pyroaurite-iowaite group: description and crystal structure. Clay Clay Miner. 55 (3), 323–334.
USEPA, 2006. In: National Primary Drinking Water Regulations. United States

Environmental Protection Agency.
van der Wens, P., Baken, K., Schriks, M., 2016. In: Bhattacharya, P., Vahter, M., Jarsjo, J., Kumpiene, J., Ahmad, A., Sparrenbom, C., Jacks, G., Donselaar, M.E., Bundschuh, J., Naidu, R. (Eds.), Arsenic at Low Concentrations in Dutch Drinking Water: Assessment of Removal Costs and Health Benefits. CRC Press, Stockholm, Sweden.
van Genuchten, C., Addy, S., Pena, J., Gadgil, A., 2012. Removing arsenic from synthetic groundwater with iron electrocoagulation: an Fe and as K-edge EXAFS study. Environ. Sci. Technol. 46 (2), 986–994.
van Genuchten, C.M., Pena, J., Amrose, S.E., Gadgil, A.J., 2014. Structure of Fe(III) precipitates generated by the electrolytic dissolution of Fe(0) in the presence of groundwater ions. Geochem. Cosmochim. Acta 127, 285–304.
van Genuchten, C., Behrends, T., Kraal, P., Stipp, S., Dideriksen, K., 2018. Controls on the formation of Fe(II,III) (hydr)oxides by Fe(0) electrolysis. Electrochim. Acta 286, 324–338.
van Genuchten, C.M., Dalby, K.N., Ceccato, M., Stipp, S.L.S., Dideriksen, K., 2017. Factors affecting the Faradaic efficiency of Fe(0) electrocoagulation. J. Environ. Chem. Eng. 5 (5), 4958–4968.
van Halem, D., Bakker, S.A., Amy, G.L., van Dijk, J.C., 2009. Arsenic in drinking water: a worldwide water quality concern for water supply companies. Drink. Water Eng. Sci. 2, 6.
Voegelin, A., Kaegi, R., Frommer, J., Vantelon, D., Hug, S.J., 2010. Effect of phosphate, silicate, and Ca on Fe(III)-precipitates formed in aerated Fe(II)- and As(III)-containing water studied by X-ray absorption spectroscopy. Geochem. Cosmochim. Acta 74 (1), 164–186.
Wan, W., Pepping, T., Banerji, T., Chaudhari, S., Giammar, D., 2011. Effects of water chemistry on arsenic removal from drinking water by electrocoagulation. Water Res. 45 (1), 384–392.
Wang, Y., Morin, G., Ona-Nguema, G., Brown, G., 2014. Arsenic(III) and arsenic(V) speciation during transformation of lepidocrocite to magnetite. Environ. Sci. Technol. 48 (24), 14282–14290.
Wang, Y., Morin, G., Ona-Nguema, G., Juillot, F., Calas, G., Brown, G., 2011. Distinctive arsenic(V) trapping modes by magnetite nanoparticles induced by different sorption processes. Environ. Sci. Technol. 45 (17), 7258–7266.
Wang, Y.H., Morin, G., Ona-Nguema, G., Juillot, F., Guyot, F., Calas, G., Brown, G.E., 2010. Evidence for different surface speciation of arsenite and arsenate on green rust: an EXAFS and XANES study. Environ. Sci. Technol. 44 (1), 109–115.
Wang, Y.H., Morin, G., Ona-Nguema, G., Menguy, N., Juillot, F., Aubry, E., Guyot, F., Calas, G., Brown, G.E., 2008. Arsenite sorption at the magnetite-water interface during aqueous precipitation of magnetite: EXAFS evidence for a new arsenite surface complex. Geochem. Cosmochim. Acta 72 (11), 2573–2586.
Waychunas, G.A., Rea, B.A., Fuller, C.C., Davis, J.A., 1993. Surface-chemistry of ferrihydrite .1. Exafs studies of the geometry of coprecipitated and adsorbed arsenate. Geochem. Cosmochim. Acta 57 (10), 2251–2269.
Webb, S., 2005. SIXPACK: a graphical user interface for XAS analysis using IFEFFIT. Phys. Scr. T115, 1011–1014.
Williams, A., Scherer, M., 2001. Kinetics of Cr(VI) reduction by carbonate green rust. Environ. Sci. Technol. 35 (17), 3488–3494.
World Health Organization, 2004. Guidelines for Drinking-Water Quality. World Health Organization, Geneva.
Wyckoff, R.W.G., 1963. Crystal Structures. Interscience Publishers, New York, New York, pp. 290–295.
Yavuz, C., Mayo, J., Yu, W., Prakash, A., Falkner, J., Yean, S., Cong, L., Shipley, H., Kan, A., Tomson, M., Natelson, D., Colvin, V., 2006. Low-field magnetic separation of monodisperse Fe3O4 nanocrystals. Science 314 (5801), 964–967.